Appl. Phys. B 70, 185–188 (2000) / Digital Object Identifier (DOI) 10.1007/s003400000183

Applied Physics B
Lasers
and Optics

Thermal effect on multiphonon-assisted anti-Stokes excited upconversion fluorescence emission in Yb^{3+}-sensitized Er^{3+}-doped optical fiber

C.J. da Silva, M.T. de Araujo, E.A. Gouveia, A.S. Gouveia-Neto

Departamento de Física, Universidade Federal de Alagoas Maceió, 57072/970, AL, Brazil
(Fax: +55-82/214-1645, E-mail: artur@fis.ufal.br)

Received: 6 April 1999/Revised version: 27 August 1999/Published online: 27 January 2000 –

Abstract. The temperature effect upon infrared-to-visible frequency upconversion fluorescence emission in Yb^{3+}-sensitized Er^{3+}-doped germanosilicate optical fibers excited with cw radiation at 1.064 μm is investigated. The experimental results revealed an eightfold enhancement in the visible upconversion emission intensity as the fiber temperature was increased from 17 °C to 180 °C. The fluorescence emission enhancement is attributed to the temperature-dependent multiphonon-assisted anti-Stokes excitation process of the ytterbium sensitizer. A theoretical approach that takes into account a sensitizer absorption cross-section, which depends on the phonon occupation number, has proven to agree very well with the experimental data

PACS: 78.20.-c; 42.79.Nv; 42.81.-i; 42.55.Wd

Frequency upconversion in rare-earth-doped optical fibers has been the subject of much interest over the past ten years owing to the possibility of developing visible superfluorescent fiber sources and visible fiber lasers excited in the near infrared [1–7]. However, for the majority of rare-earth single-doped systems the infrared-to-visible upconversion process has proven inefficient particularly for pumping in the wavelength region of 1.0 μm to 1.1 μm, where high-power sources are commercially available. The realization of Yb^{3+}-sensitized materials which exploit the efficient energy-transfer mechanism between pairs or triads of rare-earth ions, has permitted a substantial improvement in the upconversion efficiency in ytterbium-sensitized Tm^{3+} [5], Er^{3+} [6], and Pr^{3+} [8] doped optical fibers. For Yb^{3+}-sensitized codoped hosts under nonresonant excitation with the pump photon energy lower than the ytterbium $^2F_{7/2}-{}^2F_{5/2}$ transition, the upconversion pumping of the acceptor emitting levels is accomplished through multiphonon-assisted anti-Stokes excitation of the sensitizer ions [9], followed by successive energy-transfer processes. Accordingly, the effective pumping of the acceptors' luminescent excited-states is strongly dependent upon the phonon population in the host material. In this work, we demonstrate for the first time, to our knowledge, eightfold temperature-induced enhancement in the infrared-to-visible frequency upconversion efficiency of an ytterbium-sensitized erbium-doped optical fiber nonresonant pumped at 1.064 μm and heated in the temperature range of 17 °C–180 °C.

1 Experimental

The experiment was carried out using a 2.0-m length of Er^{3+}/Yb^{3+}-codoped germanosilicate optical fiber with a concentration of 8000 ppm/wt of ytterbium and 500 ppm/wt of erbium ions. The fiber had a cut-off wavelength around 1.3 μm. The excitation source was a cw Nd:YAG laser operated at 1.064 μm and ×20 uncoated microscope objectives were used to couple the pump light into it and collect the radiation emitted out from the test fiber. The fiber span temperature was increased from 17 °C to 180 °C by placing it into an aluminum oven heated by resistive wire elements. A copper–constantan thermocouple (reference at 0 °C) attached to the fiber cladding was used to monitor the temperature with ±2 °C accuracy. The signal detection and processing system consisted of a 34-cm scanning spectrograph with operation resolution of 0.5 nm equipped with a S-20 photomultiplier tube coupled to a lock-in amplifier and computer.

2 Results and discussion

Figure 1 shows typical recorded visible power spectra of radiation exiting the test fiber for a fixed pump power of 700 mW coupled into it, at two different temperatures as indicated in the plots. The spectra exhibit three distinct bands peaked around 530, 550, and 670 nm, corresponding to the $^2H_{11/2}$, $^4S_{3/2}$, and $^4F_{9/2}$ transitions to the $^4I_{15/2}$ ground-state, respectively. The less intense band around 563 nm is associated with the $^2H_{9/2}-{}^4I_{13/2}$ transition. The spectra depicted in Fig. 1 also clearly illustrate the enhancement of the infrared-to-visible upconversion efficiency as the fiber temperature was raised, at a fixed excitation power of 700 mW at 1.064 μm. The upconversion excitation mechanism responsible for the population of the visible and near-infrared emitting levels in Er^{3+}/Yb^{3+}-codoped samples excited at 1.064 μm

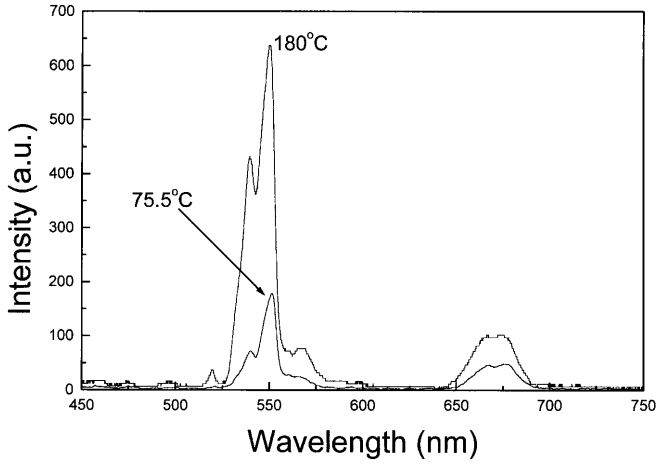

Fig. 1. Upconversion power spectra exiting the test fiber at 75 °C and 180 °C, for a fixed pump power of 700 mW at 1.064 μm

has recently been reported for silica-based optical fibers [6] and bulk glasses [10, 11]. Therefore, it suffices to mention here that the upconversion pumping process of the excited-state luminescent levels of the Er^{3+}-acceptor is obtained by means of the phonon-assisted anti-Stokes excitation of the Yb^{3+}-sensitizer or donor from the $^2F_{7/2}$ ground-state to the $^2F_{5/2}$ excited-state. The excited Yb^{3+} transfers its energy to an Er^{3+} ion, exciting it to the $^4I_{11/2}$ level, and a subsequent energy-transfer process promotes the Er^{3+} ions from the $^4I_{11/2}$ to the upper $^4F_{7/2}$ excited-state. Multiphonon-assisted nonradiative decays from the $^4F_{7/2}$ excited-state populate the $^2H_{11/2}$, $^4S_{3/2}$, and $^4F_{9/2}$ emitting levels, as it is portrayed in the simplified energy-level diagram presented in Fig. 2. The energy levels related to the 563-nm band were omitted from the diagram of Fig. 2, since throughout this work we have focused on the more intense visible bands. The excitation of the Yb^{3+}-donor from the $^2F_{7/2}$ ground-state to the $^2F_{5/2}$ excited-state, demands the participation of optical phonons in order to compensate for the energy mismatch of $\sim 800\ cm^{-1}$ between the incident pump photon at 1.064 μm (9398 cm^{-1}) and the energy connecting the $^2F_{7/2}$–$^2F_{5/2}$ transition of the ytterbium ions which is $\sim 10\,200\ cm^{-1}$. In Yb^{3+}-doped germanosilicate-based optical fibers, the inhomogeneous broadened zero-phonon absorption line is negligible beyond 1.05 μm [12]. As a consequence, the Yb^{3+} effective absorption cross-section depends upon the phonon occupation number in the host matrix, which is an increasing function of the medium temperature.

The behavior of the visible upconversion emission spectra as a function of the fiber temperature was investigated and its evolution is illustrated in Fig. 3. As can be observed, indeed there exists a steady increase in the visible emission intensities as the fiber was heated from 17 °C to 180 °C , at a fixed excitation power. Our observations can be better analyzed, when one studies the visible upconversion efficiency as a function of the fiber temperature, as indicated in the plot

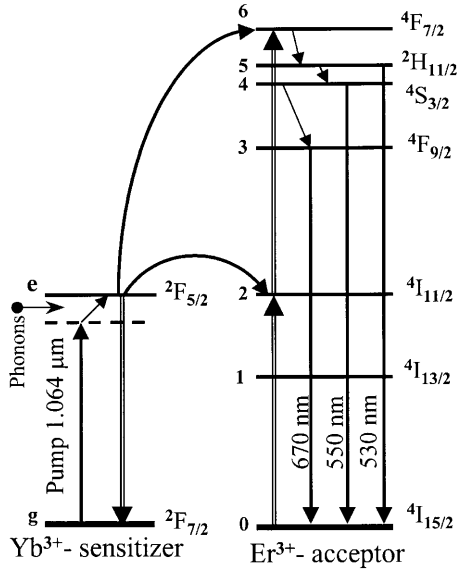

Fig. 2. Simplified energy-level diagram of the Er^{3+}/Yb^{3+} system. *Upward* and *downwards solid arrows* indicate photon absorption and emission, respectively. *Double arrows* stand for energy-transfer processes and *tilted arrows* are for multiphonon absorption and emission mechanisms

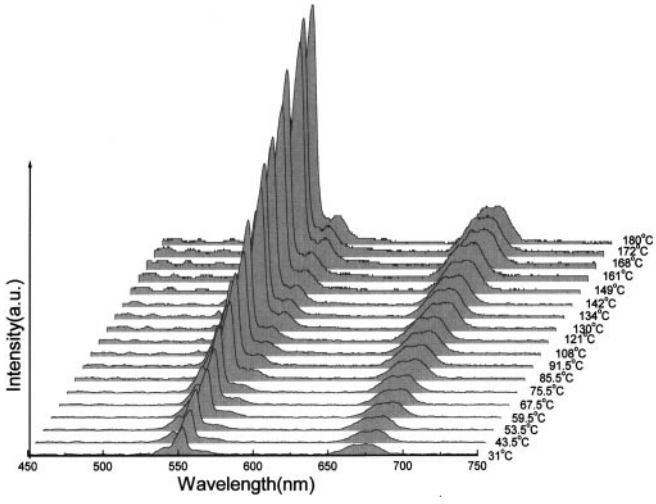

Fig. 3. Temperature evolution of the visible upconversion fluorescence emission emanating from the test fiber at a fixed excitation power of 700 mW coupled into it

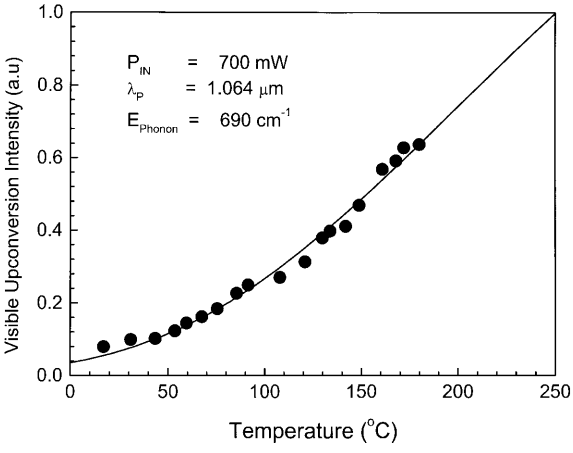

Fig. 4. Visible upconversion emission intensity as a function of temperature for a fixed excitation power of 700 mW. The *solid line* represents the theoretical curve obtained from (5) and (6), adjusted to the experimental data (*symbols*)

depicted in Fig. 4. As can be inferred from the experimental data, the integrated upconversion fluorescence intensity increased by a factor greater than eight for that range of temperature.

The experimental results shown in Figs. 3 and 4, are explained using the model portrayed in Fig. 2, and the set of rate equations needed to describe the model are listed below as in [13],

$$\dot{n}_{\mathrm{e}} = n_{\mathrm{g}}\sigma_{\mathrm{ge}}(T)\Phi + n_2 C_{2\mathrm{d}} n_{\mathrm{g}} - n_{\mathrm{e}} C_{\mathrm{d}2} n_{\mathrm{o}} - \frac{n_{\mathrm{e}}}{\tau_{\mathrm{d}}} , \tag{1a}$$

$$\dot{n}_6 = n_{\mathrm{e}} C_{\mathrm{d}6} n_2 - \frac{n_6}{\tau_6} , \tag{1b}$$

$$\dot{n}_4 = n_6 W_{64}^{\mathrm{NR}} - \frac{n_4}{\tau_4} , \tag{1c}$$

$$\dot{n}_3 = n_4 W_{43}^{\mathrm{NR}} - \frac{n_3}{\tau_3} , \tag{1d}$$

$$\dot{n}_2 = n_{\mathrm{e}} C_{\mathrm{d}2} n_{\mathrm{o}} - n_2 C_{2\mathrm{d}} n_{\mathrm{g}} - \frac{n_2}{\tau_2} , \tag{1e}$$

where $n_{\mathrm{e}} C_{\mathrm{d}i}$ ($n_2 C_{2\mathrm{d}}$) is the donor (acceptor) energy-transfer rates, which are temperature-dependent (see [14] and references therein), W_{ij}^{NR} is the nonradiative transition probability, τ_i is the level lifetime, and Φ is the power flux. In (1a)–(1e), $\sigma_{\mathrm{ge}}(T)$ represents the temperature-dependent absorption cross-section for the donor which takes into account the multiphonon-assisted sideband excitation process [9] and it is written as

$$\sigma_{\mathrm{ge}}(T) = \sigma_{\mathrm{ge}}^0 \left[\exp(\hbar\omega_{\mathrm{phonon}}/k_{\mathrm{B}}T) - 1\right]^{-p} . \tag{2}$$

In (2), σ_{ge}^0 is the absorption cross-section at resonance, $\hbar\omega_{\mathrm{phonon}}$ is the phonon energy, k_{B} is the Boltzmann constant, and T is the absolute temperature. The exponent p in (2) accounts for the number of optical phonons involved in the sensitizer excitation. The steady-state solutions for the set of (1a)–(1e) give rise to the population of the thermally coupled $^2H_{11/2}$ and $^4S_{3/2}$ emitting levels as

$$n_4 = \tau_2\tau_4\sigma_{\mathrm{ge}}^2(T) N_{\mathrm{A}} N_{\mathrm{d}}^2 C_{\mathrm{d}2} C_{\mathrm{d}6} \Phi^2 \tau_{\mathrm{d}}^2 . \tag{3}$$

In (3), N_{A} and N_{d} are the ion concentration of the acceptor and donor, respectively. In order to get the result in (3), we have assumed that the direct and back energy transfer between the acceptor and donor do not affect significantly the lifetime of the excited ions, implying that $\tau_{\mathrm{d}}^{-1} \gg n_{\mathrm{o}} C_{\mathrm{d}2}$, and $\tau_2^{-1} \gg n_{\mathrm{g}} C_{2\mathrm{d}}$ for moderate pump intensities the ground-state populations of the Yb^{3+}–Er^{3+} pair are not depleted ($n_{\mathrm{g}} \approx N_{\mathrm{d}}$, $n_{\mathrm{o}} \approx N_{\mathrm{A}}$). Furthermore, the excited-state level $^4F_{7/2}$ of Er^{3+} decays simply nonradiatively to $^2H_{11/2}$ and $^4S_{3/2}$ levels, and multiphonon decay from $^2F_{7/2}$ level of Yb^{3+} is not expected due to the large energy separation to the ground-state so that, τ_{d} is mainly radiative. The observed energy separation between the $^2H_{11/2}$ and $^4S_{3/2}$ levels was $\Delta E_{45} \approx 700\,\mathrm{cm}^{-1}$, which allows thermal population of the $^2H_{11/2}$ level. Correspondingly, the radiative decay time τ_4^{R} of the $^4S_{3/2}$ level is temperature-dependent through

$$\frac{1}{\tau_4^{\mathrm{R}}} = \frac{\sum_j A(^4S_{3/2} \to j) + 3\mathrm{e}^{-\Delta E_{45}/k_{\mathrm{B}}T} \sum_j A(^2H_{11/2} \to j)}{1 + 3\mathrm{e}^{-\Delta E_{45}/k_{\mathrm{B}}T}} , \tag{4}$$

where $A(^2H_{11/2},\ ^4S_{3/2} \to j)$ are radiative transitions rates from the two to the lower lying levels, and the effective populations for the coupled levels are

$$n_4^{\mathrm{eff}} = n_4 \frac{1}{1 + 3\mathrm{e}^{-\Delta E_{45}/k_{\mathrm{B}}T}} , \tag{5a}$$

$$n_5^{\mathrm{eff}} = n_4 \frac{3\mathrm{e}^{-\Delta E_{45}/k_{\mathrm{B}}T}}{1 + 3\mathrm{e}^{-\Delta E_{45}/k_{\mathrm{B}}T}} . \tag{5b}$$

Finally, with the proper substitution, the visible emission intensity is obtained through the relation

$$I_{\mathrm{visible}} = \sum_i I_i = \hbar \sum_i \omega_{i\mathrm{o}} A_{i\mathrm{o}} n_i . \tag{6}$$

Based upon these calculations, we need the temperature-dependent lifetimes for the participant levels and also the nonradiative transition probabilities. The nonradiative transition probability between levels i and j for low concentration of Er^{3+} ions (our case) is due to multiphonon relaxation processes, and can be related to the temperature by means of the following expression [15]

$$W_{ij}^{\mathrm{NR}}(T) = W_{ij}^{\mathrm{NR}}(0) \left[1 - \exp(-\hbar\omega_{\mathrm{phonon}}/k_{\mathrm{B}}T)\right]^{-p} , \tag{7}$$

where $W_{ij}^{\mathrm{NR}}(0)$ is its value at zero temperature. Actually, this probability can be obtained in two ways: subtracting the radiative transition probability (calculated by the Judd–Ofelt theory [16, 17]) from the inverse of the observed lifetime or by direct measurement. Furthermore, the energy of the $^4I_{11/2}$ excited level of Er^{3+} is approximately half of the $^4F_{7/2}$ level and nearly resonant to the $^2F_{5/2}$ level of Yb^{3+}, which implies that the temperature dependence of the energy transfer rates $C_{\mathrm{d}i}$ from Yb^{3+} to Er^{3+} is mainly due to the overlap integrals between the emission of the ytterbium and the absorption of the erbium [18]. However, in several glasses and crystals, the effect of the temperature increase upon the green and red emission of the Er^{3+}, after resonant excitation of the Yb^{3+} sensitizer, is in the direction of the visible light intensity decrease for the range of temperatures above 20 °C [19]. Hence, the temperature dependence of the upconversion visible light emission associated with the overlap integrals could not account for the temperature behavior exhibited in our findings. The major contribution to the results herein presented is then attributed to the temperature dependence of the ytterbium absorption cross-section as displayed in (2), and without lack of generality the temperature dependence of the overlap integrals could be neglected in our calculations. Using the calculated radiative transition probabilities for silicate glasses [20], and nonradiative decay rates for silica-based glasses [21], we have obtained the temperature dependence of the emission intensities of the three visible emission bands as well as of the total visible upconversion emission with the resultant curves indicated by the solid line in the plot of Fig. 4. Indeed, the theoretical model based upon the temperature dependence residing ìn the effective absorption cross-section of the ytterbium sensitizer describes quite well our experimental observations for the individual emission intensities at 530, 550, and 670 nm and the integrated visible upconversion emission efficiency. Moreover, the same model has also been applied to ytterbium-sensitized Er^{3+}-doped chalcogenide and Pr^{3+}-doped fluoroindate glasses and

has also proven to agree very well with the experimental data, as described elsewhere [22, 23]. An alternative approach to explain our results would be the possibility that thermal enhancement of the population in the highest lying Stark sublevels of the ytterbium ground-state manifold would give an important contribution to the temperature dependence of the upconversion emission enhancement. However, when one describes the system using only a Boltzmann factor, the theoretical results deviate rapidly from the experimental data for temperatures above 135 °C. The thermal population of the highest Stark sublevels of course produces some enhancement in the upconversion process, but certainly the temperature dependence of the sensitizer absorption cross-section through the multiphonon-asssisted anti-Stokes excitation process is the dominant mechanism.

From the results presented in Fig. 2, we have also obtained the energy of $\sim 690\,\mathrm{cm}^{-1}$ for the phonon-mode participating in the multiphonon-assisted anti-Stokes excitation of the sensitizer. This result is to be compared with the one of $1100\,\mathrm{cm}^{-1}$ for the maximum phonon-energy associated with silica-based glass [20, 21, 24]. The deviation in the value for the phonon energy obtained in our measurements, and the maximum value of $1100\,\mathrm{cm}^{-1}$, is due to the fact that in anti-Stokes sideband excitation processes one has to consider an "effective-phonon-mode", which has a much lower energy than the host cut-off value [24]. At high temperatures the population distribution of the phonons participating in the excitation process is centered around this low energy "effective-phonon-mode", as demonstrated both experimentally and theoretically by Auzel and Chen for Er^{3+}-doped ZBLAN and silica glasses [24]. On the other hand, the highest phonon frequency of the host is the one that minimizes the multiphonon order in radiationless emission processes [25, 26].

3 Conclusions

In conclusion, we have demonstrated both theoretically and experimentally a times eight thermally induced enhancement in the infrared-to-visible upconversion efficiency in an Er^{3+}/Yb^{3+}-codoped germanosilicate optical fiber excited at 1.064 μm. The eightfold efficiency enhancement was obtained by heating the fiber in the temperature range of 17 °C to 180 °C, and was attributed to the temperature-dependent multiphonon-assisted sideband excitation process of the Yb^{3+} sensitizer. The theoretical analysis utilizing rate equations, and considering the absorption cross-section of the sensitizer as a function of the phonon occupation number of the host, has proven to agree quite well with experimental data. Our results suggest that this technique can be exploited to improve output powers and reduce threshold of rare-earth (Pr, Er, and Tm) doped glasses and fiber lasers sensitized with ytterbium and pumped by high-power sources in the 1.0-μm wavelength region as has recently been demonstrated for an Er^{3+}/Yb^{3+}-codoped germanosilicate optical fiber laser [27]. In addition, it can be used to improve the performance, by reducing the inherent thermal noise at high temperatures of optical temperature-sensing devices based upon upconversion flourescence emission in Er^{3+}/Yb^{3+}-codoped glasses and fibers pumped at 1.064 μm [28–30].

Acknowledgements. The financial support for this work by FINEP (Financiadora de Estudos e Projetos), CNPq (Conselho Nacional de Desenvolvimento Científico e Tecnológico), CAPES (Coordenadoria de Aperfeiçoamento de Pessoal de Ensino Superior) and PADCT (Programa de Apoio ao Desenvolvimento Científico e Tecnológico), and PRONEX-NEON (UFPE/UFAL/UFPB) is gratefully acknowledged. The research of Carlos Jacinto da Silva is supported by an undergraduate studentship from the PIBIC/CNPq/UFAL (Programa Institucional de Bolsas de Iniciação Científica).

References

1. T.F. Carruthers, I.N. Duling III, C.M. Shaw, E.J. Friebele: Appl. Phys. Lett. **54**, 875 (1989)
2. R.M. Percival, M.W. Phillips, D.C. Hanna, A.C. Tropper: IEEE J. Quantum Electron. **QE-25**, 2119 (1989)
3. J.Y. Allain, M. Monerie, H. Poignant: Electron. Lett. **26**, 261 (1990); ibid **26**, 166 (1990)
4. A.S.L. Gomes, C.B. de Araujo, B.J. Ainslie, S.P. Craig-Ryan: Appl. Phys. Lett. **57**, 2169 (1990)
5. D.C. Hanna, R.M. Percival, I.R. Perry, R.G. Smart, J.E. Townsend, A.C. Tropper: Opt. Commun. **78**, 187 (1990)
6. Y-M. Hua, Q. Li, Y.L. Chen, Y.X. Chen: Opt. Commun. **88**, 441 (1992)
7. D.L. Nicácio, E.A. Gouveia, A.M. Reis, N.M. Borges, A.S. Gouveia-Neto: IEEE J. Quantum Electron. **QE-30**, 2634 (1994)
8. J.Y. Allain, M. Monerie, H. Poignant: Electron. Lett. **27**, 1156 (1991)
9. F. Auzel: Phys. Rev. B **13**, 2809 (1976)
10. A.S. Oliveira, M.T. de Araujo, A.S. Gouveia-Neto, A.S.B. Sombra, J.A. Medeiros Neto, N. Aranha: J. Appl. Phys. **83**, 604 (1998)
11. A.S. Oliveira, M.T. de Araujo, A.S. Gouveia-Neto, A.S.B. Sombra, J.A. Medeiros Neto, Y. Messaddeq: Appl. Phys. Lett. **72**, 753 (1998)
12. R. Paschotta, J. Nilsson, A.C. Tropper, D.C. Hanna: IEEE J. Quantum Electron. **QE-33**, 1049 (1997)
13. J.C. Wright: Top. Appl. Phys. **15**, 239 (1976)
14. F. Auzel: Proc. IEEE **61**, 758 (1973)
15. M.J. Weber: Phys. Rev. B **8**, 54 (1973)
16. B.R. Judd: Phys. Rev. **127**, 750 (1962)
17. G.S. Ofelt: J. Chem. Phys. **37**, 511 (1962)
18. T. Miyakawa, D.L. Drexter: Phys. Rev. B **1**, 2961 (1970)
19. D.C. Yeh, W.A. Sibbey, M. Suscavage, M.G. Drexhage: J. Appl. Phys. **62**, 266 (1987)
20. J.A. Capobianco, G. Prevost, P.P. Proulx, P. Kabro, M. Bettinelli: Opt. Mater. **6**, 175 (1996)
21. C.B. Layne, W.H. Lowdermilk, M.J. Weber: Phys. Rev. B **16**, 10 (1977)
22. P.V. dos Santos, C.J. da Silva, E.A. Gouveia, M.T. de Araujo, A.S. Gouveia-Neto, A.S.B. Sombra: Proceedings of the International Conference on Luminescence and Optical Spectroscopy of Condensed Matter – ICL'99 – Osaka, Japan, paper B01-5 (1999)
23. A.S. Oliveira, E.A. Gouveia, M.T. de Araujo, A.S. Gouveia-Neto, C.B. de Araujo, Y. Messaddeq: Proceedings of the International Conference on Luminescence and Optical Spectroscopy of Condensed Matter – ICL'99 – Osaka, Japan, paper PC3-3 (1999)
24. F. Auzel, Y.H. Chen: J. Lumin. **66**/**67**, 224 (1996)
25. E. Okamoto, H. Masui, K. Muto, K. Awazu: J. Appl. Phys. **43**, 2122 (1973)
26. M.D. Shinn, W.A. Sibbley, M.G. Drexhage, R.N. Brown: Phys. Rev. B **27**, 6635 (1983)
27. C.J. da Silva, M.T. de Araujo, E.A. Gouveia, A.S. Gouveia-Neto: Opt. Lett. **24**, 1287 (1999)
28. H. Berthou, C.K. Jorgensen: Opt. Lett. **15**, 1100 (1990)
29. P.V. dos Santos, M.T. de Araujo, A.S. Gouveia-Neto, J.A. Medeiros Neto, A.S.B. Sombra: Appl. Phys. Lett. **73**, 578 (1998)
30. P.V. dos Santos, M.T. de Araujo, A.S. Gouveia-Neto, J.A. Medeiros Neto, A.S.B. Sombra: IEEE J. Quantum Electron. **QE-35**, 395 (1999)